CHEMICAL ENGINEERING TRANSACTIONS
VOL. 56, 2017
A publication of AIDIC
The Italian Association of Chemical Engineering
Online at www.aidic.it/cet
Guest Editors: Jiří Jaromír Klemeš, Peng Yen Liew, Wai Shin Ho, Jeng Shiun Lim

ISBN 978-88-95608-47-1; **ISSN** 2283-9216
DOI: 10.3303/CET1756189

Syngas Production from Combined Steam and Carbon Dioxide Reforming of Methane over Ce-modified Silica-supported Nickel Catalysts

Tan Ji Siang[a], Huong T. Danh[b], Sharanjit Singh[a], Quang Duc Truong[c], Herma Dina Setiabudi[a], Dai-Viet N. Vo*[,a,d]

[a]Faculty of Chemical & Natural Resources Engineering, University Malaysia Pahang, Lebuhraya Tun Razak, Gambang 26300, Pahang, Malaysia
[b]Clean Energy and Chemical Engineering, Korea University of Science and Technology (UST), Daejeon, 305-350, Korea
[c]Institute of Multidisciplinary Research for Advanced Materials, Tohoku University Katahira 2-1-1, Aoba-Ku, Sendai 980-8577, Japan
[d]Centre of Excellence for Advanced Research in Fluid Flow, Universiti Malaysia Pahang, 26300 Gambang, Kuantan, Pahang, Malaysia
vietvo@ump.edu.my

This study investigates the physicochemical attributes of Ce-modified Santa Barbara Amorphous-15 (SBA-15) supported Ni catalyst and evaluates its catalytic performance for combined steam and CO_2 reforming of methane in order to produce synthesis gas. Both 10 % Ni/SBA-15 and 10 % Ni/Ce-SBA-15 catalysts were prepared by conventional wetness impregnation method and characterised via Brunauer-Emmett-Teller (BET) surface area, H_2 temperature-programmed reduction (H_2-TPR) and X-ray diffraction (XRD) techniques. Both 10 % Ni/Ce-SBA-15 and 10 % Ni/SBA-15 catalysts possessed high BET surface area of 595.04 $m^2\ g^{-1}$ and 493.73 $m^2\ g^{-1}$. XRD measurement revealed the existence of NiO phase with crystallite sizes of 15.5 nm and 13.6 nm for the corresponding 10 % Ni/SBA-15 and 10 % Ni/Ce-SBA-15 catalysts whilst cerium (IV) oxide (CeO_2) particles were well dispersed on the mesoporous SBA-15 support surface. H_2-TPR results showed that NiO to Ni^0 reduction was completely obtained at temperature beyond 800 K and the reduction temperature was contingent on the degree of metal-support interaction associated with size and location of NiO nanoparticles on support. Ce-modified catalyst was more stable and active than unmodified Ni/SBA-15 catalyst. 10 % Ni/Ce-SBA-15 catalyst exhibited a significant enhancement in CH_4 conversion (up to 11.06 %) and H_2 yield (30.51 mol%) reasonably due to the high oxygen storage capacity and redox property of CeO_2 phase incorporated into the mesoporous framework of SBA-15 support. H_2/CO ratio of 10 % Ni/Ce-SBA-15 catalyst was stable at about 1.74 while a lower value of 1.14 was observed for 10 % Ni/SBA-15 catalyst indicating the occurrence of parallel reactions including CH_4 steam reforming reaction and CH_4 dry reforming reaction.

1. Introduction

Although carbon-rich fossil fuels such as coal, crude oil and natural gas are the main energy sources and play an important role in industrial production as well as economic development, the combustion of fossil fuels unavoidably induces global warming and climate change due to excessive greenhouse gas emissions. Synthesis gas or syngas referring to a mixture of H_2 and CO has been regarded as a potential and green alternative for petroleum-based energy (Usman et al., 2015) since it is currently utilised as a feedstock for Fischer-Tropsch synthesis (FTS) to yield gasoline range hydrocarbons (Vo and Adeshina, 2012). The conventional approaches for syngas production are partial oxidation, dry or steam reforming of methane (Usman et al., 2015). Combined steam and CO_2 reforming of methane (CSCRM) has recently gained significant interests from both academia and industry since it mitigates CO_2 emission by converting it to value-added syngas with a desirable H_2/CO ratio close to 2 which is known as a practical feed composition for FTS

Please cite this article as: Siang T.J., Danh H.T., Singh S., Truong Q.D., Setiabudi H.D., Vo D.V.N., 2017, Syngas production from combined steam and carbon dioxide reforming of methane over ce-modified silica-supported nickel catalysts, Chemical Engineering Transactions, 56, 1129-1134 DOI:10.3303/CET1756189

(Jang et al., 2016). The other advantage of CSCRM is the capable production of flexible H_2/CO ratios via manipulation of CH_4/CO_2/H_2O feed composition. CSCRM is a complex process involving multiple reactions including steam reforming of methane, CO_2 reforming of methane and water-gas shift (WGS) reactions as seen in Eq(1)-(3).

$$CH_4 + H_2O \rightarrow 3H_2 + CO \quad (\Delta H^o_{298K} = +206\ kJ\ mol^{-1}) \tag{1}$$

$$CH_4 + CO_2 \rightarrow 2H_2 + 2CO \quad (\Delta H^o_{298K} = +247\ kJ\ mol^{-1}) \tag{2}$$

$$CO + H_2O \leftrightarrow H_2 + CO_2 \quad (\Delta H^o_{298K} = -41\ kJ\ mol^{-1}) \tag{3}$$

For the reforming reactions of hydrocarbons, nickel-containing catalysts have been conventionally employed owing to their excellent capability for C-H and C-C bonds rupture, low cost and highly global availability (Da Silva et al., 2014). The serious problem related with Ni-based catalysts is the rapid catalytic deactivation due to carbonaceous deposition and sintering effect at high reduction and reaction temperature (Liu et al., 2012). A large number of studies have been carried out recently to develop more stable nickel-based catalysts with high coke resistance for reforming reactions. CeO_2 promoter reportedly increased the strength of metal-support interaction and supplied active oxygen for coke removal from catalyst surface due to its great redox property (Maestri et al., 2009). The addition of CeO_2 dopant to Ni/SBA-15 catalyst reportedly enhanced remarkably the catalytic activity and stability for oxidative dehydrogenation of ethane (Shi et al., 2008) and methane steam reforming reactions (Wang et al., 2009). As there was no previous study about the role of CeO_2 addition on Ni/SBA-15 catalyst for CSCRM reaction. The aim of this study was to examine the physicochemical properties of Ce-incorporated SBA-15 supported Ni catalyst and its catalytic performance for CSCRM reaction.

2. Experimental

2.1 Catalyst preparation

Siliceous SBA-15 support was synthesised using a hydrothermal synthesis method. A calculated amount of triblock-poly(ethylene glycol)-block-poly(propylene glycol)-block-poly(ethylene glycol), also known as P-123 ($EO_{20}PO_{70}EO_{20}$) was initially dissolved in HCl solution with a controlled pH value of about one at 313 K. This mixture was then stirred for two hours to ensure the complete dissolution of P-123 triblock copolymer before the addition of tetraethyl orthosilicate (TEOS) followed by rigorously stirring at the similar temperature for 24 hours. The hydrothermal treatment was subsequently carried out in a Teflon-lined autoclave at 373 K for 24 hours. The resulting white solid powder was filtered and washed with distilled water until the pH of about 4 was achieved. After it was dried in an oven at 323 K overnight, air-calcination at 823 K was conducted for the dried solid sample with a heating rate of two K min^{-1} for 5 h. A similar procedure was also implemented for synthesising a 5 % Ce - 95 % SBA-15 support, except that Cerium(III) nitrate hexahydrate ($Ce(NO_3)_3.6H_2O$) solution was introduced together with the addition of TEOS into the P-123 triblock copolymer mixture.
Both 10 % Ni/SBA-15 and 10 % Ni/Ce-SBA-15 catalysts were prepared by a conventional wetness impregnation method between the corresponding SBA-15 and Ce-SBA-15 supports with $Ni(NO_3)_2.6H_2O$ as a metallic precursor. A precise quantity of Ni $(NO_3)_2.6H_2O$ aqueous solution was impregnated with as-synthesised SBA-15 or Ce-SBA-15 supports and magnetically stirred at room temperature for 3 h followed by drying in an oven at 373 K overnight and calcination in flowing air at 1,073 K with a ramping rate of 2 K min^{-1} for 5 h.

2.2 Catalyst characterisation

The measurement of Brunauer-Emmett-Teller (BET) surface area for support and catalyst was conducted in a Micromeritics ASAP-2010 apparatus using N_2 physisorption at 77 K. Prior to measurement, all samples were purged in N_2 flow for 1 h at 573 K for moisture and contaminant removal. X-ray diffraction (XRD) measurements were carried out in a Rigaku Miniflex II system using Cu monochromatic X-ray radiation with wavelength, λ of 1.5418 Å operating at 30 kV and 15 mA. Relatively small scan speed and step size of corresponding 1° min^{-1} and 0.02° were implemented during scanning within the 2θ range of 3° to 80° in order to achieve high-resolution patterns. Scherrer's formula (Patterson, 1939) was used for computing the average crystallite size of NiO phase, *d(NiO)*. The Ni^0 metallic particle size, $d(Ni^0)$ after the H_2 reduction of NiO particles was roughly estimated based on the relative molar volumes of metallic Ni^0 and NiO phases (cf. Eq(4)) (Baum, 1998). The metallic dispersion, *D* was calculated using Eq(5) by assuming the spherical shape of Ni^0 particles (Xu et al., 2009).

$$d(Ni^0) = 0.84d(NiO) \quad (4)$$

$$D(\%) = \frac{90\,nm}{d(Ni^0)} \quad (5)$$

The AutoChem II-2920 system was used for conducting H_2 temperature-programmed reduction (H_2-TPR). Catalyst sample was pre-treated at 373 K for 30 min in 50 mL min^{-1} of He inert gas, followed by reduction step in flowing 10 % H_2/Ar mixture (50 mL min^{-1}) from 373 to 1,173 K with a heating rate of 10 K min^{-1}. A scanning electron microscope (SEM, SU-6600, HITACHI) and an energy dispersive X-ray spectrometer (EDX, Incas-act, Oxford Instruments) were also used to characterise catalyst.

2.3 Combined steam and CO_2 reforming of methane reaction

The CSCRM reaction was performed under atmospheric pressure at 1,073 K in a quartz tube fixed-bed continuous flow reactor (O.D. = 3/8 in. and length, *L* = 17 in.) for 10 h using about 0.1 g of catalyst mounted by quartz wool in the middle of reactor. KellyMed KL-602 syringe pump was used to feed purified water to the top of reactor in which it was subsequently vaporised before being mixed with CH_4 and CO_2 reactants (reactant partial pressure, P_{CH4} = 40 kPa and P_{CO2} = P_{H2O} = 20 kPa) previously diluted in a mixer with N_2 gas. N_2 diluent gas is acting as a tie component for material balance purpose and guaranteeing the constant total flow rate of 60 mL min^{-1} for each run. High gas hourly space velocity, GHSV of 36 L g_{cat}^{-1} h^{-1} was implemented for all runs to ensure the absence of internal and external transport resistances. The composition of gaseous effluent from the bottom of fixed-bed reactor was analysed in an Agilent 6890 Series GC system using TCD detector. The catalytic performance for the CSCRM reaction was evaluated according to methane conversion, X_{CH4} and H_2 yield, Y_{H2} as shown in Eq(6) and (7).

$$X_{CH_4}(\%) = \frac{F_{CH_4}^{In} - F_{CH_4}^{Out}}{F_{CH_4}^{In}} \text{ x } 100\ \% \quad (6)$$

$$Y_{H_2}(\%) = \frac{2F_{H_2}^{Out}}{4F_{CH_4}^{In} + 2F_{H_2O}^{In}} \text{ x } 100\ \% \quad (7)$$

where F^{In} and F^{out} are the corresponding inlet and outlet molar flow rates ($mole^{-1}$).

3. Results and discussion

3.1 Physicochemical properties

3.1.1 Textural properties

The textural characteristic of mesoporous SBA-15 and Ce-SBA-15 supports as well as Ni-based catalysts is summarised in Table 1. Both SBA-15 and Ce-SBA-15 supports possessed high BET surface area of about 780 and 760 m^2 g^{-1}. The similar total pore volume and average pore diameter for these supports would suggest the insignificant change in textural structure of SBA-15 support with Ce addition. The successful incorporation of NiO nanoparticles into the mesoporous frameworks of SBA-15 and Ce-SBA-15 supports resulted in an unavoidable decrease in BET surface area, total pore volume and average pore diameter for both 10 % Ni/SBA-15 and 10 % Ni/Ce-SBA-15 catalysts in agreement with findings from Wang et al. (2012).

Table 1: Textural properties of supports and Ni-based catalysts.

Sample	BET specific surface area (m^2 g^{-1})	Total pore volume (cm^3 g^{-1})[a]	Average pore diameter (nm)[b]
SBA-15	780.09	1.35	6.94
Ce-SBA-15	760.47	1.21	6.66
10 % Ni/SBA-15	493.73	0.97	6.69
10 % Ni/Ce-SBA-15	595.04	1.08	6.38

[a] Total pore volume obtained at p/p^0 = 0.99.

[b] Average pore diameter calculated by Barret-Joyner-Halenda (BJH) desorption method.

3.1.2 X-ray diffraction measurement

Figure 1 (a) shows the XRD patterns of fresh mesoporous 10 % Ni/Ce-SBA-15 and 10 % Ni/SBA-15 catalysts. A similar broad diffraction peak at 2θ angle of around 23° observed in the X-ray diffractograms of both

catalysts was assigned to the amorphous SiO2 phase of SBA-15 framework (Landau et al., 2005). The similar XRD patterns for SiO2 phase of 10 % Ni/Ce-SBA-15 and 10 % Ni/SBA-15 catalysts would further emphasise that the mesoporous structure of SBA-15 support was unchanged with embedded Ce metal oxide. As seen in Figure 1, four high intensive sharp peaks on the diffractograms of both catalysts identified at 2θ of 37.46°, 43.54°, 63.03° and 75.14° were attributed to the corresponding (1 1 1), (2 0 0), (2 2 0) and (3 1 1) crystal planes of NiO phase (JCPDS card No. 47-1049). The characteristic peaks of CeO2 phase were not identified in XRD measurement (Figure 1 (a)) but Ce element was detected by SEM-EDX analysis (Figure 1(b)). This observation suggested that CeO2 particles were well incorporated into the mesoporous framework of SBA-15 support or Si atoms in the silica framework were isomorphously substituted by Ce atoms. CeO2 nanoparticles may be formed with a considerably small crystallite size below the detection limit of XRD measurement. The average crystallite size of NiO particles for both 10 % Ni/Ce-SBA-15 and 10 % Ni/SBA-15 catalysts were about 13.60 and 15.54 nm, respectively computed from the most intense NiO line at 2θ of 43.54° by Scherrer's equation. The Ni^0 metallic particle dimension and metal dispersion for 10 % Ni/Ce-SBA-15 catalyst were estimated as ca. 11.42 nm and 7.88 %, correspondingly whilst for 10 % Ni/SBA-15 catalyst, particle size of Ni0 active metal and metal dispersion were about 13.05 nm and 6.90 % in that order.

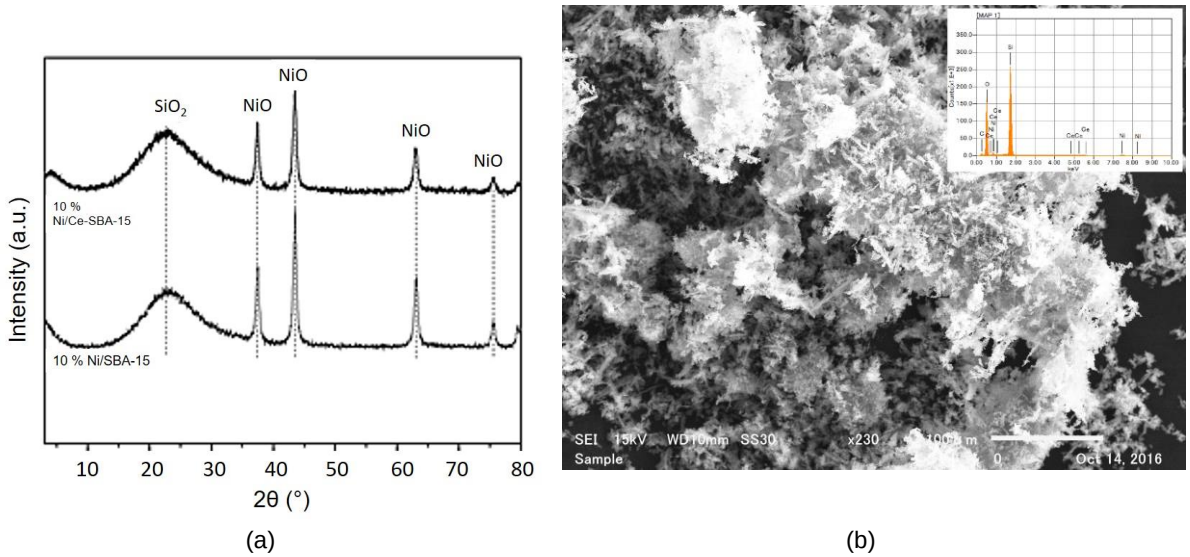

Figure 1: (a) XRD patterns of fresh 10 % Ni/Ce-SBA-15 and 10 % Ni/SBA-15 catalysts; and (b) SEM-EDX spectrum for 10 % Ni/Ce-SBA-15 catalyst

3.1.3 H_2 temperature-programmed reduction

Figure 2 shows the H_2-TPR profiles of 10 % Ni/SBA-15 and 10 % Ni/Ce-SBA-15 catalysts with 10 % H_2/Ar mixture. Although NiO reduction was widely recognised as a single process for Ni^0 metallic phase formation without the involvement of an intermediate metal oxide (Foo et al., 2012), two noticeable broad peaks were evident for both catalysts in this study. According to He et al. (2009), nickel silicate phase was reportedly reduced at high temperature above 973 K which is higher than the observed peaks in H_2-TPR profiles for both catalysts (Figure 2). XRD measurements (Figure 1) did not detect the appearance of nickel silicate for these catalysts. Both peaks in H_2-TPR were assigned to the reduction of NiO to Ni^0 metallic phase and the extent of metal-support interaction depending on crystallite size and the location of NiO particles on mesoporous support was responsible for the formation of multiple reduction peaks. The high temperature peak was due to the reducibility of small NiO nanoparticles embedded in the mesoporous channels of siliceous supports with a strong interaction between metal and support (Kim et al., 2015) whilst the low temperature peak corresponded to the reduction of larger surface NiO particles possessing a weak metal-support interaction (Oemar et al., 2016).

3.2 Catalytic activity and stability evaluation

A 10 h on-stream stability test was performed for both 10 % Ni/SBA-15 and 10 % Ni/Ce-SBA-15 catalysts to examine their catalytic performance and stability for CSCRM reaction. As seen in Figure 3, both CH_4 conversion and H_2 yield were improved by 11.06 % and 30.51 %, respectively with Ce-modification on SBA-15 support reasonably due to higher metal dispersion. The Ce-modified SBA-15 supported Ni catalyst appeared

to be more stable than 10 % Ni/SBA-15 catalyst for 10 h on-stream rationally owing to the excellent redox property and high oxygen storage capacity of CeO_2, facilitating gasification process of carbonaceous species, C_xH_y (Eq(8) and (9)) on catalyst surface (Wang et al., 2006).

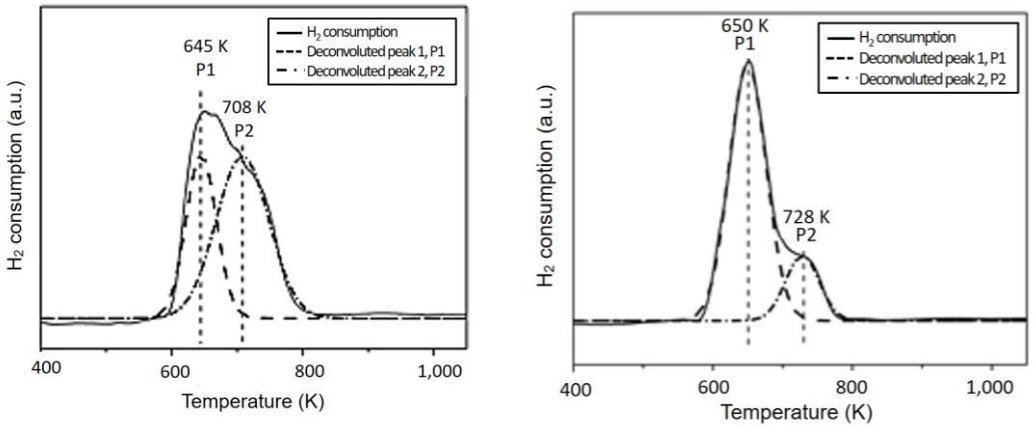

(a) (b)

Figure 2: H_2-TPR profiles of (a) 10 % Ni/SBA-15 and (b) 10 % Ni/Ce-SBA-15 catalysts at a heating rate of 10 K min^{-1}.

$$2xCeO_2 + C_xH_y \rightarrow xCe_2O_3 + xCO + 0.5yH_2 \quad (8)$$

$$Ce_2O_3 + 5CO_2 \rightarrow 2CeO_4 + 5CO \quad (9)$$

As seen in Figure 3 (b), the H_2/CO ratio of 10 % Ni/Ce-SBA-15 catalyst was stable at about 1.74 whereas a lower value of 1.14 was observed for 10 % Ni/SBA-15. The H_2/CO ratio varied within 1 to 2 for both catalysts was appropriate for long-chain hydrocarbon production from FTS and indicative of the occurrence of parallel reactions, i.e., CH_4 steam reforming and CH_4 dry reforming reactions. CH_4 steam reforming yielded a H_2/CO ratio of 3 whilst a lower H_2/CO ratio of less than 1 was obtained from CH_4 dry reforming reaction (Usman et al., 2015). The presence of both reactions resulted in the ratio of H_2/CO within 1 to 2.

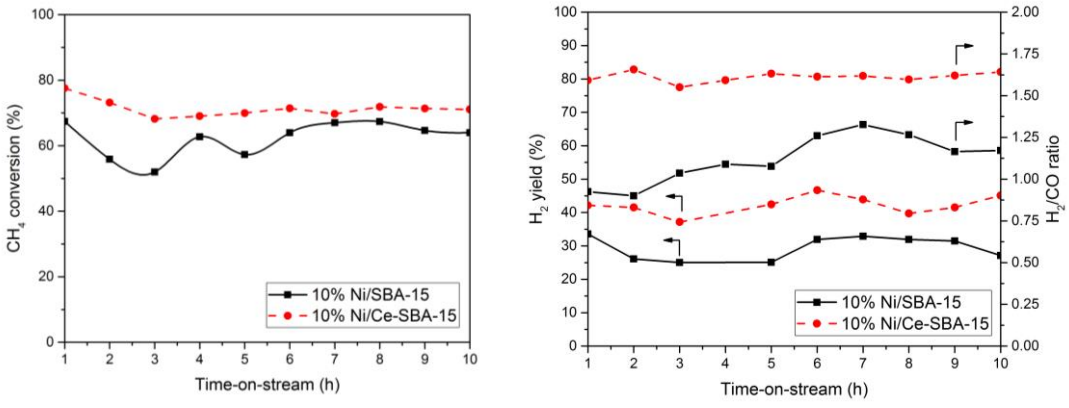

(a) (b)

Figure 3: Effect of Ce-modified SBA-15 support on (a) CH_4 conversion and (b) H_2 yield and H_2/CO ratio with time-on-stream at PCH_4 = 40 kPa, PCO_2 = PH_2O = 20 kPa and 1,073 K.

4. Conclusions

Both 10 % Ni/SBA-15 and 10 % Ni/Ce-SBA-15 catalysts synthesised by the wetness impregnation method was evaluated for CSCRM reaction in a quartz fixed-bed reactor at P_{CH4} = 40 kPa, P_{CO2} = P_{H2O} = 20 kPa, 1,073 K and 1 atm. The 10 % Ni/SBA-15 and 10 % Ni/Ce-SBA-15 catalysts possessed high BET surface area ranging from 493.73-595.04 m^2 g^{-1}. The XRD and SEM-EDX measurements suggested that CeO_2 particles

were effectively embedded into the ordered mesoporous SBA-15 framework while H_2-TPR profiles indicated that the reduction of NiO nanoparticles was a single process and the crystallite dimension of these particles was less than 15.5 nm for both catalysts. The catalytic performance of 10 % Ni/Ce-SBA-15 catalyst was always higher and more stable than 10 % Ni/SBA-15 catalyst in terms of CH_4 conversion and H_2 yield rationally due to the redox property and excellent oxygen storage capacity of CeO_2. The H_2/CO ratio obtained for both catalysts was always between the range of 1 and 2 desirable for high molecular weight hydrocarbon production from downstream FTS.

Acknowledgments

The authors are grateful for the financial support from Universiti Malaysia Pahang via UMP Research Grant Scheme (RDU160323) to conduct this study.

References

Baum E.J., 1998, Chemical property estimation: Theory and application, Lewis Publishers, Boca Raton, US.

Da Silva A.L.M., den Breejen J.P., Mattos L.V., Bitter J.H., de Jong K.P., Noronha, F.B., 2014, Cobalt particle size effects on catalytic performance for ethanol steam reforming - Smaller is better, J. Catal 318, 67-74.

Foo S.Y., Cheng C.K., Nguyen T.-H., Kennedy E.M., Dlugogorski B.Z., Adesina A.A., 2012, Carbon deposition and gasification kinetics of used lanthanide-promoted Co-Ni/Al_2O_3 catalysts from CH_4 dry reforming, Catal. Communn. 26, 183-188.

He S., Jing Q., Yu W., Mo L., Lou H., Zheng X., 2009, Combination of CO_2 reforming and partial oxidation of methane to produce syngas over Ni/SiO_2 prepared with nickel citrate precursor, Catal. Today 148, 130-133.

Jang W.-J., Jeong D.-W., Shim J.-O., Kim H.-M., Roh H.-S., Son I.H., Lee S.J., 2016, Combined steam and carbon dioxide reforming of methane and side reactions: Thermodynamic equilibrium analysis and experimental application, Appl. Energy 173, 80-91.

Kim D., Kwak B.S., Min B.-K., Kang M., 2015, Characterization of Ni and W co-loaded SBA-15 catalyst and its hydrogen production catalytic ability on ethanol steam reforming reaction, Appl. Surf. Sci. 332, 736-746.

Landau M.V., Vradman L., Wang X., Titelman L., 2005, High loading TiO_2 and ZrO_2 nanocrystals ensembles inside the mesopores of SBA-15: Preparation, texture and stability, Microporous and Mesoporous Mater. 78, 117-129.

Liu D., Wang Y., Shi D., Jia X., Wang X., Borgna A., Lau R., Yang Y., 2012, Methane reforming with carbon dioxide over a Ni/ZiO_2–SiO_2 catalyst: Influence of pretreatment gas atmospheres, Int. J. Hydrogen Energy 37, 10135-10144.

Maestri M., Vlachos D., Beretta A., Forzatti P., Groppi G., Tronconi E., 2009, Dominant reaction pathways in the catalytic partial oxidation of CH_4 on Rh, Top. Catal. 52, 1983-1988.

Oemar U., Kathiraser Y., Mo L., Ho X.K., Kawi S., 2016, CO_2 reforming of methane over highly active La-promoted Ni supported on SBA-15 catalysts: mechanism and kinetic modelling, Catal. Sci. & Technol. 6, 1173-1186.

Patterson A.L., 1939, The Scherrer formula for X-ray particle size determination, Phys. Rev. 56, 978-982.

Shi X., Ji S., Wang K., 2008, Oxidative dehydrogenation of ethane to ethylene with carbon dioxide over Cr–Ce/SBA-15 catalysts, Catal. Lett. 125, 331-339.

Usman M., Daud W.M.A.W., Abbas H.F., 2015, Dry reforming of methane: Influence of process parameters-A review, Renew. Sustain. Energy Rev. 45, 710-744.

Vo D.-V.N., Adesina A.A., 2012, A potassium-promoted Mo carbide catalyst system for hydrocarbon synthesis, Catal. Sci. Technol. 2, 2066-2076.

Wang K., Li X., Ji S., Shi X., Tang J., 2009, Effect of $Ce_xZr_{1-x}O_2$ promoter on Ni-based SBA-15 catalyst for steam reforming of methane, Energy and Fuel 23, 25-31.

Wang N., Chu W., Zhang T., Zhao X.S., 2012, Synthesis, characterization and catalytic performances of Ce-SBA-15 supported nickel catalysts for methane dry reforming to hydrogen and syngas, Int. J. Hydrogen Energy 37, 19-30.

Wang X., Rodriguez J.A., Hanson J.C., Gamarra D., Martínez-Arias A., Fernández-García M., 2006, In situ studies of the active sites for the water gas shift reaction over Cu-CeO_2 catalysts: Complex interaction between metallic copper and oxygen vacancies of ceria, J. Phys. Chem. B. 110, 428-434.

Xu J., Chen L., Tan K.F., Borgna A., Saeys M., 2009, Effect of boron on the stability of Ni catalysts during steam methane reforming, J. Catal. 261, 158-165.